ACCEPTED ARTICLE PREVIEW

Accepted Article Preview: Published ahead of advance online publication

Laser optothermal nanobomb for efficient flattening of nanobubbles in van der Waals materials

Jia-Tai Huang, Benfeng Bai Hong-Ren Chen, Peng-Yi Feng, Jian-Yu Zhang, Yu-Xiao Han, Xiao-Jie Wang, Hong-Wei Zhou, Yuan Chai, Yi Wang, Guan-Yao Huang, Hong-Bo Sun

Cite this article as: Jia-Tai Huang, Benfeng Bai Hong-Ren Chen, Peng-Yi Feng, Jian-Yu Zhang, Yu-Xiao Han, Xiao-Jie Wang, Hong-Wei Zhou, Yuan Chai, Yi Wang, Guan-Yao Huang, Hong-Bo Sun. Laser optothermal nanobomb for efficient flattening of nanobubbles in van der Waals materials. *Light: Advanced Manufacturing* accepted article preview 10 December, 2025; doi: 10.37188/lam.2026.007

This is a PDF file of an unedited peer-reviewed manuscript that has been accepted for publication. LAM are providing this early version of the manuscript as a service to our customers. The manuscript will undergo copyediting, typesetting and a proof review before it is published in its final form. Please note that during the production process errors may be discovered which could affect the content, and all legal disclaimers apply.

Received 16 January 2025; revised 27 November 2025; accepted 10 December 2025;
Accepted article preview online 10 December 2025

Accepted Manuscript

ACCEPTED ARTICLE PREVIEW

Laser optothermal nanobomb for efficient flattening of nanobubbles in van der Waals materials

Jia-Tai Huang[1], Benfeng Bai[1,], Hong-Ren Chen[1], Peng-Yi Feng[1], Jian-Yu Zhang[1], Yu-Xiao Han[1], Xiao-Jie Wang[1], Hong-Wei Zhou[1], Yuan Chai[1], Yi Wang[1], Guan-Yao Huang[2], Hong-Bo Sun[1,*]*

[1] *State Key Laboratory of Precision Measurement Technology and Instruments, Department of Precision Instrument, Tsinghua University, Beijing 100084, China*

[2] *Key Laboratory for Thermal Science and Power Engineering of Ministry of Education, Beijing Key Laboratory of CO_2 Utilization and Reduction Technology, Department of Energy and Power Engineering, Tsinghua University, Beijing 100084, China.*

Corresponding to: baibenfeng@tsinghua.edu.cn;hbsun@tsinghua.edu.cn.

KEYWORDS: van der Waals material, nanodefect, laser modification, optothermal effect;

Abstract

Nanobubbles are typical nanodefects commonly existing in two-dimensional (2D) van der Waals materials such as transition metal dichalcogenides, especially after their transfer from growth substrate to target substrates. These nanobubbles, though tiny, may significantly alter the local electric, optoelectronic, thermal, or mechanical properties of 2D materials and therefore are rather detrimental to the constructed devices. However, there is no post-processing method so far that can effectively eliminate nanobubbles in 2D materials after their fabrication and transfer, which has been a major obstacle in the development of 2D material based devices. Here, we

Accepted Manuscript

propose a principle, called laser optothermal nanobomb (LOTB), that can effectively flatten nanobubbles in 2D materials through a dynamic process of optothermally induced phase transition and stress-pulling effect in nanobubbles. Operation of LOTB on monolayer molybdenum disulfide (1L-MoS_2) films shows that the surface roughness can be reduced by more than 70% on a time scale of ~50 ms, without damage to the intrinsic property of 1L-MoS_2 as validated by micro-nano photoluminescence and Raman spectroscopy. Moreover, a dual-beam cascaded LOTB and a multi-shot LOTB strategies are proposed to increase the flattened area and processing effect, showing the potential of LOTB for fast nanodefect repairing in the mass production of van der Waals materials and devices.

Introduction

Two-dimensional (2D) van der Waals (vdW) materials, such as transition metal dichalcogenides (TMDs),[1, 2] have emerged as important candidate materials for next-generation chip-scale optoelectronic devices.[3-6] However, due to the restriction of growth at high temperatures (>500 °C) [7] and the different thermal expansion coefficients of 2D materials and growth substrates,[8] 2D materials have to be transferred from growth substrates to target substrates after growth, during which various nanodefects such as nanobubbles are inevitably generated.[9] Nanobubbles, though very tiny with dimensions typically from 10 nm to 1 μm,[10, 11] may significantly alter the dielectric environment[12, 13] and tensile strain[14, 15] of 2D materials and therefore are rather detrimental to the excitonic properties, band gap structures, and carrier mobility of the composed devices.[4, 6, 15] Some previous works have tried to reduce the impact of nanobubbles by developing clean transfer methods.[16] Although those pre-processing methods can reduce the occurrence of nanobubbles to some extent, it does not always completely eliminate the nanobubbles formed during the transfer process.[16] Therefore, the post-processing methods are required to address the residual nanobubbles. Different from the pre-processing methods, the post-processing methods commonly involve

Accepted Manuscript

selective and localized elimination of the residual nanobubbles without affecting the global properties of the material. However, there is no post-processing method so far that can effectively eliminate nanobubbles in 2D materials, due to the vdW interactions between 2D materials and substrates.

In essence, nanobubbles are generated in 2D vdW materials due to the unexpected inclusion of impurities during their growth or transfer. Therefore, the key to removing nanobubbles is to drive away the inclusions. Previous research has shown that large-area annealing can help to improve the adhesion between TMD films and substrates.[17] However, this method just drives small nanobubbles to merge as fewer but larger bubbles instead of eliminating them. Rosenburger et *al*. proposed to eliminate bubbles mechanically by pushing bubble inclusions laterally with an atomic force microscope (AFM) probe.[18] Since the probe needs to contact sample during treatment, it lacks efficiency and is only applicable to some substrates such as hexagonal boron nitride but not to hard substrates such as silica. Therefore, a high-efficiency, reliable, and versatile nanobubble elimination method is highly expected.

Here, we report an all-optical method named laser optothermal nanobomb (LOTB), which can effectively eliminate nanobubbles in 2D materials such as TMDs on a short time scale of ~50 ms by laser beam irradiation, without material damage to the intrinsic optoelectronic properties of materials. The focused laser beam induces an optothermal effect on the nanobubble, which triggers the phase transition of the inclusions in nanobubbles into gas, sublimates the 2D material film to generate a tiny sacrifice breach, and then drives the inclusion to flow out of the bubble through the breach under pressure difference. This effect can be analogized to a central hole formed by a bomb explosion, accompanied by the flattening of the surrounding area. As a demonstration, LOTB is employed to eliminate nanobubbles in monolayer molybdenum disulfide (1L-MoS_2). On this basis, by regulating the irradiated optical field, a dual-beam cascaded LOTB and a multi-shot LOTB strategies are proposed to expand the treatment areas and improve the processing effectiveness.

Accepted Manuscript

Results

Mechanics of nanobubble formation. The formation of nanobubble in a 2D material film can be described by a modified pressurized membrane model.[19] As shown in Fig. 1a (i), denoting the height and radius of the nanobubble as h and $a = (A/\pi)^{0.5}$, where A represents the bottom area of the nanobubble, the aspect ratio of nanobubbles is calculated by h/a. Further, a nanobubble can be regarded as the deflection of a pressurized membrane. Its profile can be expressed as

$$w(r) = h(1 - \frac{r^2}{a^2}), \quad (1)$$

where w is the deflection at a radial distance of r from the center. The bending energy of the membrane is negligible due to the thinness of the 2D materials.[11] The total free energy consists of the stretching energy U_s and the adhesion energy U_i. Considering the membrane structure in equilibrium, the mechanical relationship can be determined by minimizing the total free energy ($U_s + U_i$). The aspect ratio of a nanobubble can be calculated as (see details in Supporting Information, Note 1)

$$h/a \propto (\Delta\gamma / K)^{1/4}, \quad (2)$$

where $\Delta\gamma$ is the adhesion energy per unit area and K is the in-plane elastic stiffness.

The mechanical and optoelectronic properties of nanobubbles are influenced by both the film-substrate interfacial interaction and the trapped inclusions inside. When nanobubbles arise after wet transfer, liquids such as water may be trapped inside the nanobubbles.[4] Previous research has shown that the adsorbed water is the most likely inclusion in nanobubbles and liquid-free interfaces of transferred 2D materials are possible only when the transfer is performed above 110 °C.[20]

For a liquid-filled nanobubble, the adhesion energies of the membrane-liquid interface, substrate-liquid interface, and membrane-substrate interface need to be considered, which can be written in the form below based on Young-Dupré equation[21]

$$\Delta\gamma = \Gamma - \gamma_c(\cos\theta_f + \cos\theta_s), \quad (3)$$

Accepted Manuscript

where Γ is the adhesion energy between the membrane and substrate, γ_c is the surface tension of the inclusion (whose value for water is around 0.078 J/m^2), and θ_f and θ_s are the contact angles on the membrane and on the substrate, respectively.

For a gas-filled nanobubble, $\Delta\gamma$ can be simply taken as the adhesion energy of the membrane-substrate interface, i.e., $\Delta\gamma = \Gamma$. By taking into account Eq. (2) and Eq. (3), we know that the aspect ratio of a gas-filled nanobubble is larger than that of a liquid-filled one with the same membrane and substrate. According to the minimum total free energy principle, the pressure difference Δp inside and outside a nanobubble can be derived as (see details in Supporting Information, Note 1)

$$\Delta p = 16(1+v)\frac{D}{a^3}\frac{h}{a} + \frac{4}{3}\frac{K}{a}\left(\frac{h}{a}\right)^3, \tag{4}$$

where $D = Et^3/12(1-v^2)$ is the flexural rigidity of the film, E is the Young's modulus, t is the thickness of film, and v is the Poisson ratio.

Principle of LOTB. Based on the above mechanical analysis of nanobubbles, we propose the LOTB method whose physical process is schematically depicted in Fig. 1a. For the nanobubbles commonly generated during the wet-transfer process of 2D materials, their contents can initially be regarded as liquid water. A detailed analysis of the nanobubble contents is provided by combining the mechanical model with the specific experimental situation in Supporting Information, Note 6. When a focused continuous-wave (CW) laser beam irradiates a single layer TMD (1L-TMD) film with liquid-filled nanobubbles, a light-induced temperature field is generated over the film, which consists of a high-temperature (high-temp) field region and a low-temperature (low-temp) field region. In the central region of the beam, the high-temp field sublimates the 1L-TMD film to generate a sacrifice breach so that the inclusion of the nanobubble can flow out of the bubble. While in the low-temp field region, the

Accepted Manuscript

inclusion evaporates from liquid phase to gas phase and flows to the high-temp region under the inner pressure $p = p_0 + \Delta p$, where p_0 is the atmospheric pressure outside and Δp is a pressure difference. In this way, the inclusion of nanobubble can escape from the film in the form of gas through the sacrifice breach driven by pressure difference. As a result, the nanobubbles in the low-temp field can be flattened by paying the little price of generating a small sacrifice breach.

The optothermal process depicted in stage (ii) of Fig. 1a is justified by numerical simulation with finite element method (COMSOL Multiphysics), where an example material system of monolayer MoS_2 (1L-MoS_2) on a silica substrate is considered (see simulation details in Supporting Information, Note 2). As shown in Fig. 1b, under irradiation by a Gaussian laser beam with an intensity (power density) of 106.1 mW/μm^2 and beam diameter of 0.3 μm (green line, normalized), the simulated temperature profile (black line) has a peak temperature around 900 K and a wider full width at half maximum (FWHM) compared to the laser spot due to the heat diffusion effect. By taking into account the sublimation temperature point of 1L-MoS_2 (723 K) and the boiling point of water (373 K), the high-temp field region (red) and low-temp field region (blue) can be identified, which have a radius of 0.18 μm (r_H) and a radius of 0.98 μm (r_L). Accordingly, the areas of the sacrifice region and flattened region can be estimated as 0.10 μm^2 ($S_s = \pi r_H^2$) and 2.90 μm^2 ($S_F = \pi r_H^2 - \pi r_L^2$), respectively. The mechanism assumes that the liquid inside the bubble has the properties of bulk water. Considering the water inside the nanobubble trapped under pressure, it has a higher boiling point compared to that at atmospheric pressure, which may induce a decrease in the radius of the flattened region.[22, 23]

In addition to the phase transition, the stress-pulling effect induced by the expansion of nanobubbles under laser irradiation can help to flatten the film. Since the position of Raman peaks reflects the strain situation of the 1L-TMDs and the E_{2g}^1 and A_{1g} peaks of 1L-MoS_2 will red shifts under strain,[24, 25] detailed Raman studies were

Accepted Manuscript

carried out to experimentally confirm the enhancement of strain and stress on expanded nanobubble under laser irradiation. As shown in Fig. S1b, The Raman spectra from the nanobubble area (solid curves) and nearby flat area (dashed curves) on a 1L-MoS_2 film under high-power (2 mW, red curves) and low-power (0.2 mW, blue curves) irradiation lasers was measured to confirm the stress-induced Raman shift. The extra Raman red shift on the nanobubble area (ΔE_{2g}^1 = 2 cm^{-1}, ΔA_{1g} = 1 cm^{-1}) proves the existence of increased stress on nanobubble under laser irradiation. According to previous reports,[23] the ratio of the E_{2g}^1 shift concerning strain is about 3.2 cm^{-1}/% in CVD-grown 1L-MoS_2,[26] which calculates the increasing strain equals around 0.63% in this nanobubble by dividing the extra shift of E_{2g}^1 by this ratio. The detailed simulation and Raman measurement was discussed in Supporting Information, Note 3.

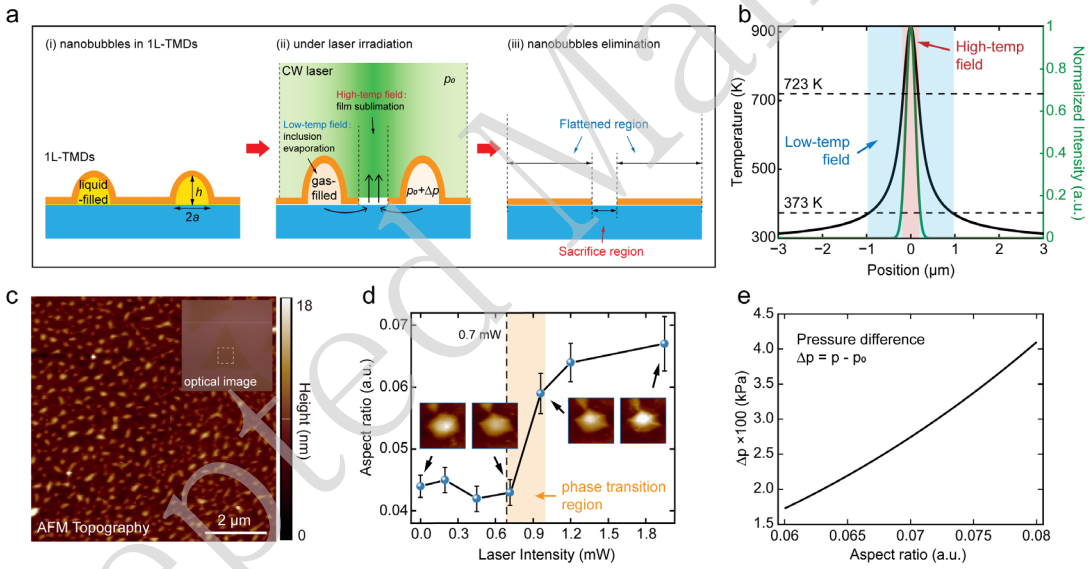

Figure 1. Principe of LOTB. (a) Schematic diagram of the bubble flattening process with LOTB. In stage (i), liquid-filled nanobubbles are generated during wet transfer; in stage (ii), a high-temp field region and a low-temp field region are generated under laser irradiation, which sublimates the TMD film to generate a sacrifice region and enables the phase transition of the inclusions, respectively; in stage (iii), the inclusions inside the nanobubbles flow out of the sacrifice region under the pressure difference inside and outside nanobubbles, which flattens the film together with a stress-pulling effect.

Accepted Manuscript

(b) Simulated temperature distribution (black line) under the irradiation of a Gaussian laser beam (green line, normalized) with an intensity of 106.1 mW/μm^2 and beam diameter of 0.3 μm. The red and blue regions indicate the high-temp field and low-temp field regions, respectively. (c) AFM topography of a transferred 1L-MoS_2 sample with nanobubbles. The inset shows the optical image of the 1L-MoS_2 film, where the dashed rectangle indicates the region of the AFM topography. (d) Aspect ratio change of a nanobubble under different irradiation laser power, where the orange area indicates the phase transition region leading to an abrupt change of aspect ratio and the black dashed line indicates the power threshold. The insets show the corresponding AFM topography images of the same nanobubble under different irradiation laser powers. (e) Calculated pressure difference inside and outside the nanobubble versus the aspect ratio. The radius of the nanobubble is taken as 200 nm.

Dynamic change of nanobubbles under laser irradiation. To investigate the dynamic change of nanobubbles under laser irradiation experimentally, 1L-MoS_2 samples were prepared by chemical vapor deposition (CVD) and transferred onto glass coverslips by KOH-based wet transfer method[27] (see Methods section for details). As the AFM topography images show in Fig. 1c, many nanobubbles with radii of 50 nm ~ 400 nm and heights of 2 nm ~ 16 nm were generated, which are too small to be observed by optical microscope in the inset.[4] Based on our previous work, the as-grown sample films did not exhibit a similarly widespread distribution of nanobubbles, indicating that these nanobubbles are formed during the wet-transfer process.[4] The aspect ratio of nanobubbles can be estimated as ~0.04 according to the statistics of the nanobubble topography, similar to the case of liquid-filled blister with the material system of MoS_2/SiO_2 reported before.[11] The detailed analysis of the liquid-filled nanobubbles was discussed in Supporting Information, Note 6.

Then we illuminate the film with a focused laser beam. The 1L-MoS_2 is a direct bandgap semiconductor, exhibiting edge band absorption properties, which can absorb

Accepted Manuscript

photons with energies above their optical bandgap as the absorption spectrum shown in Fig. S5. The wavelength of the laser was selected as 532 nm to correspond to the side absorption band of 1L-MoS_2 so that the laser energy can be efficiently absorbed and generate the temperature field distribution. The change of the aspect ratio of a nanobubble with a radius of around 200 nm under increasing irradiation laser power was measured by an AFM, as shown in Fig. 1d. The process is clearly divided into three stages: when the laser power is relatively low, the aspect ratio of the nanobubble changes very little; when the laser power increases and reaches the threshold power of ~0.7 mW (indicated by the black dashed line in Fig. 1d) and remains within the range of 0.7 ~ 0.96 mW (marked by the orange rectangle in Fig. 1d), the aspect ratio increases sharply; and after that, the aspect ratio increases slowly. The error bars presented in Fig. 1d indicate the measurement uncertainty of the aspect ratio, which was quantified via single-point measurements and subsequent error propagation analysis (see Supporting Information, Note 8 for details). Since the laser acts as a heating source to linearly raise the temperature of the film and its inclusions with the increase of the laser power, the orange region indicates a phase transition region of the inclusions. That is, the liquid inclusion evaporates into gas so that the liquid-filled nanobubble is turned into a gas-filled one with higher aspect ratio. After that, when the laser power is further increased to 2 mW, the temperature of the gas-filled nanobubble continues to rise, leading the increase of the internal pressure and the further increase of the aspect ratio. This fact is consistent with the simulation result that the aspect ratio is nearly proportional to the temperature in a gas-filled nanobubble shown in Fig. S2 (see details in Supporting Information, Note 4). Moreover, according to the measured aspect ratio curve in Fig. 1d, the pressure difference Δp inside and outside a nanobubble with respect to aspect ratio can be calculated by Eq. (4) and plotted in Fig. 1e.

Accepted Manuscript

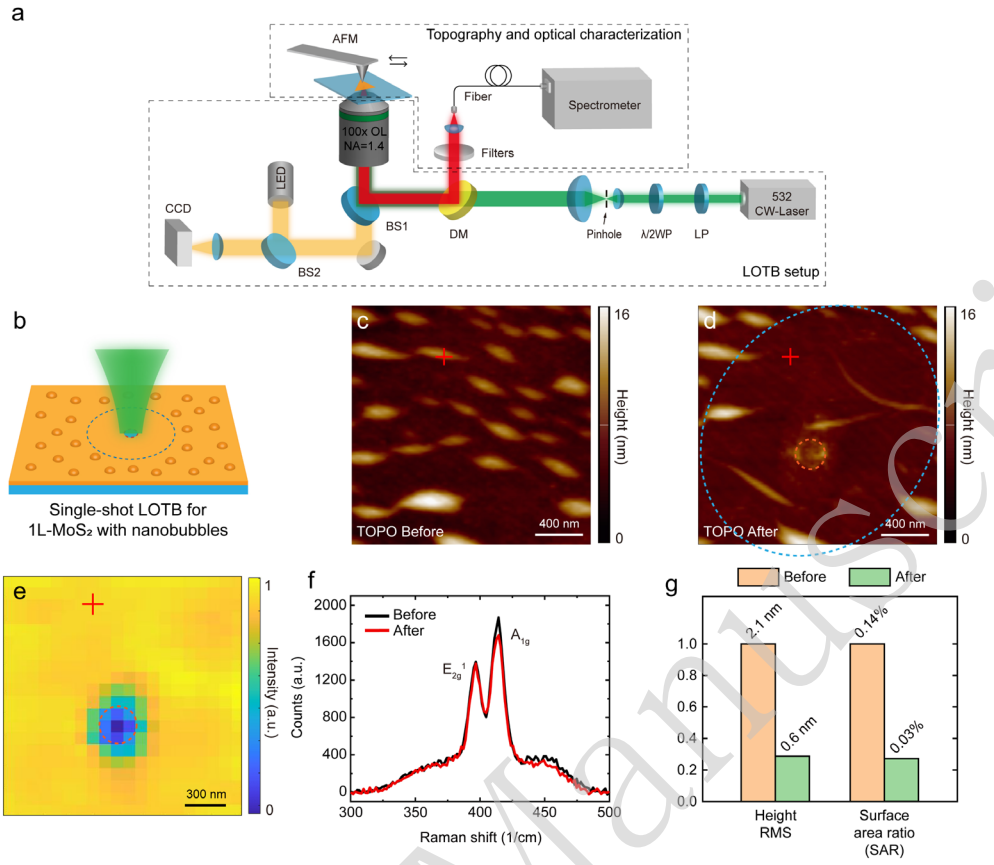

Figure 2. Elimination of nanobubbles in 1L-MoS_2 by single-shot LOTB. (a) Schematic of the LOTB setup, which can be used jointly with an AFM and an optical spectroscopic characterization system. (b) Schematic of nanobubble flattening on a 1L-MoS_2 sample by single-shot LOTB. (c) and (d) are AFM topography images of a 1L-MoS_2 sample with nanobubbles before and after LOTB treatment, respectively. The orange and blue dashed lines indicate the sacrifice region and the flattened region, respectively. (e) Confocal PL mapping image of the same sample area as in (d) after LOTB. (f) Raman spectra of the sample before (black curve) and after (red curve) LOTB treatment at the point marked by the red cross in (c)-(d). (g) Surface roughness statistics of the flattened region before and after LOTB.

Single-shot LOTB for nanobubble elimination. An instrumental setup has been built to implement LOTB, as schematically shown in Fig. 2a, which can be used jointly with an AFM and an optical spectroscopic characterization system. A 532 nm CW laser

Accepted Manuscript

of 7.5 mW power is used to illuminate the sample from bottom side through an oil-immersed objective lens (100x, 1.4 NA, Olympus). Since the temperature distribution is directly induced by the irradiated optical field as the simulation result in Fig. 1b, the size of the sacrifice region can be controlled by simply adjusting the laser spot size, such as employing objective lenses with different NA, altering the divergence angle of the incident laser beam, or shifting the focal plane. And the diameter of the laser spot is ~0.3 μm. The AFM probe can be aligned precisely with the laser spot. All the experiments were carried out in ambient and the detailed system information is described in Methods section.

The LOTB can be performed with single shot to eliminate the nanobubbles in 1L-MoS_2, as schematically shown in Fig. 2b. Figures 2c and 2d show the topography changes of the same 1L-MoS_2 sample area before and after LOTB treatment, respectively. The sample used is a triangular flake with a side length of ~25 μm. Clearly, a small sacrifice region is generated in the center (orange dashed line), around which nanobubbles are eliminated and the film is obviously flattened (blue dashed line). The diameters of the sacrifice region and the flattened region are measured to be ~0.3 μm and ~2 μm, respectively, which are consistent with the simulation results in Fig. 1b. As a result, the surface roughness of the film is reduced, which can be quantified by calculating the root mean square (RMS) of topography after laser irradiation. As shown in Fig. 1g, the RMS is reduced by 71% (from 2.1 nm to 0.6 nm). The residual wrinkles may formed by the directional movement and convergence of nanobubbles' inclusion under laser irradiation,[28, 29] which was discussed in Supporting Information, Note 9.

Moreover, since the inclusions inside nanobubbles cause deformation of the 1L-MoS_2, we may define a surface area ratio $\mathrm{SAR} = \iint (\mathrm{d}S - S_P)/S_P$ to quantify the presence of the inclusions, where S_P represents the projection area of the flattened region. The smaller the value of SAR, the closer the film is attached to the substrate without inclusions. As shown in Fig. 1g, the SAR decreases by 79% (from 0.14% to 0.03%) after laser irradiation, indicating that the inclusions indeed disappear instead of

Accepted Manuscript

shifting or converging as the situation in annealing.[17] The flattening effect of the LOTB is also influenced by the location of laser irradiation and the original spatial distribution of adjacent nanobubbles. The experiment of the single-shot LOTB in different flakes and irradiation regions shown in Fig. S8 demonstrates the effectiveness of the LOTB method under various irradiation conditions (see details in Supporting Information, Note 10). Besides, the LOTB method was proved also effective in other substrates including the commonly used hBN substrate in 2D devices as shown in Fig. S9.

In order to identify whether the 1L-MoS_2 film was damaged in material properties, especially optical properties, after LOTB, we performed micro-nano photoluminescence (PL) and Raman spectral characterizations of the sample to investigate the change of its properties, including the optoelectric property, electronic energy band, and vibrational modes.[4, 30] The PL and Raman spectral results in Figs. 2e and 2f show that the 1L-MoS_2 film was intact after LOTB. Despite the PL quenching in the sacrifice region in Fig. 2e, the PL emission intensity in the flattened region is even and as strong as that in the surrounding region nearby. The Raman spectra were measured at the same point as shown in Fig. 2f, which has nearly no change in intensity and peak position, indicating that LOTB does not damage the material properties in the flattened region.

The time scale of LOTB was investigated by carrying out experiments with different treatment time under the same power 6 mW through the transistor-transistor logic (TTL) modulation of the CW laser source. As shown in Fig. S13 in Supporting Information, the effect of nanobubble elimination appears at 20 ms and becomes evident after 50 ms (see details in Supporting Information, Note 15). Furthermore, to rule out the field effect and shock wave by laser, we have carried out a similar experiment using a single picosecond laser as shown in Fig. S14 in Supporting Information, which shows no flattening effect in both AFM topography (see details in Supporting Information, Note 16). Besides, the long-term stability (> 13 months) of the

Accepted Manuscript

LOTB-treated regions was confirmed through topography measurement shown in Fig. S15.

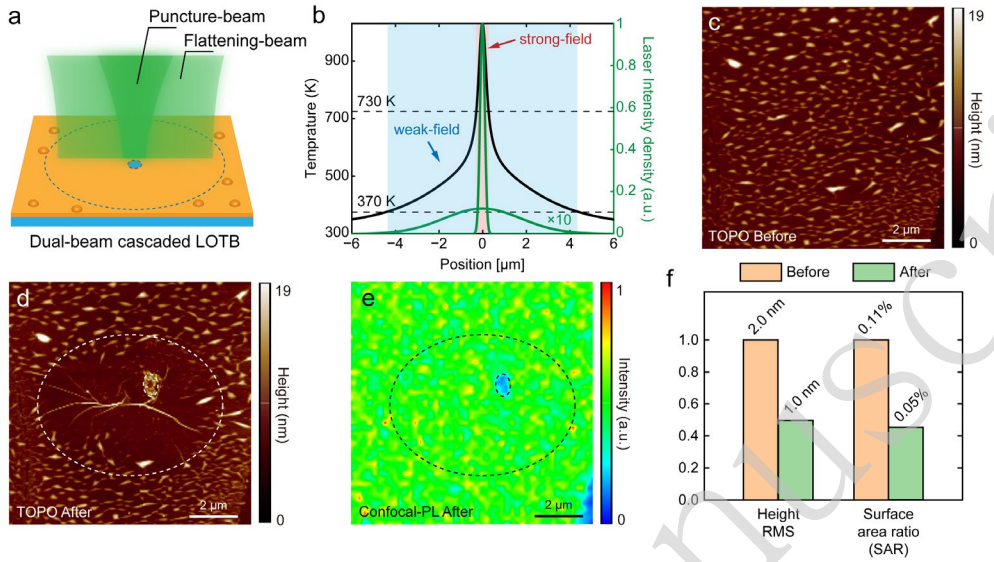

Figure 3. Dual-beam cascaded LOTB. (a) Schematic of implementing the dual-beam cascaded LOTB. A strong puncture-beam has a smaller diameter and high-intensity while a relatively weak flattening-beam has a larger diameter and low-intensity, which control the high-temp and low-temp field regions, respectively. (b) Simulated temperature distribution (black line) under the irradiation of two Gaussian lasers (green lines), consisting of a puncture-beam (with an intensity of 106.1 mW/μm^2 and a spot diameter of 0.3 μm) and a flattening-beam (with an intensity of 1.3 mW/μm^2 and a spot diameter of 5 μm). The red and blue regions indicate the high-temp field region and low-temp field region, respectively. (c) and (d) are AFM topography images of a 1L-MoS_2 sample with nanobubbles before and after the dual-beam cascaded LOTB treatment, respectively. The dashed lines indicate the sacrifice region and flattened region. (e) Confocal PL mapping images of the same sample area as that in (d) after laser irradiation. (f) Surface roughness statistics of the flattened region before and after LOTB.

Accepted Manuscript

Dual-beam cascaded LOTB and multi-shot LOTB. The single-shot LOTB uses a single Gaussian laser beam to generate both the high-temp and low-temp field regions, which limits the area and position of the flattened region. In fact, the two fields can be controlled by separate laser beams or multi-shot irradiation. In this way, we have developed a dual-beam cascaded LOTB and a multi-shot LOTB to increase the treatment area and effect.

Figure 3a shows the schematic diagram of the dual-beam cascaded LOTB, where a narrow puncture-beam and a wide flattening-beam are used to simultaneously irradiate the sample. As the simulation results in Fig. 3b show (see simulation details in Supporting Information, Note 2), the two green lines indicate the two beam profiles with Gaussian distribution: one has a smaller diameter (0.3 μm) and higher intensity (106.1 mW/μm^2) and one has a larger diameter (5 μm) and lower intensity (1.3 mW/μm^2). While the puncture-beam generates the high-temp field region, the flattening-beam plays a role in increasing the range of the low-temp field region by decreasing the gradient of the optical and temperature fields in the center. The black line indicates the simulated in-plane temperature distribution. Compared to the distribution in Fig. 1b with single-shot LOTB, the range of the high-temp field region (red) remains nearly unchanged with a radius of 0.28 μm while the range of the low-temp field region (blue) is 4.3 times larger with a radius of 4.35 μm, determining a 20.4 times lager flattened region as 59.2 μm^2.

The instrumental setup of the dual-beam cascaded LOTB and the laser spot of two beams are shown in Fig. S16 in Supporting Information, Note 18. The power of the puncture-beam is 7.5 mW that is the same as the single-shot case, and the power of the flattening-beam is 25 mW. Figures 3c and 3d show the AFM topography changes of the sample film before and after LOTB treatment. The diameters of the sacrifice and flattened regions are measured to be ~0.4 um and ~6 um, consistent with the simulation results in Fig. 3b. The flattened region is around 9.2 times larger than that in the single-shot LOTB in Fig. 2. The surface roughness of the film is also investigated, as shown

Accepted Manuscript

in Fig. 3f, where the height RMS and SAR are decreased by 50% and 55%, respectively. The smaller roughness reduction can be attributed to the stress-pulling effect since the stress decays with the square of the distance in space as derived in Supporting Information, Note 3. The results also indicate that the phase transition effect is dominant in LOTB with the assistance of the stress-pulling effect. As a comparison, the nanobubbles remain unchanged when irradiating the film with only the puncture-beam as shown in Fig. S18 in Supporting Information, proving that the flattening effect in Fig. 3d is indeed the combined effect of the two beams.

To investigate the property of the treated film, confocal PL mapping was conducted and shown in Fig. 3e. Similar to the results in Fig. 2d, the confocal PL mapping reveals that the emission intensity in the flattened region is even and as strong as the surrounding area nearby, indicating that the dual-beam cascaded LOTB does not damage the material properties in the flattened region. Besides, the flattening effect can be further improved by converting the flattening-beam into a flat-top profile through the beam shaper.[31]

As the results of dual-beam cascaded LOTB, the scalability of the LOTB method could be enhanced by enlarger the spot size of the flattening-beam, which can be realized by simply adjusting the optical path such as replacing the lens with a shorter focal length or repositioning the lens. On the other hand, the throughput of the LOTB method can be further improved by thermal treatments such as global annealing and using multifocal parallel irradiation strategies such as microlens arrays.

Accepted Manuscript

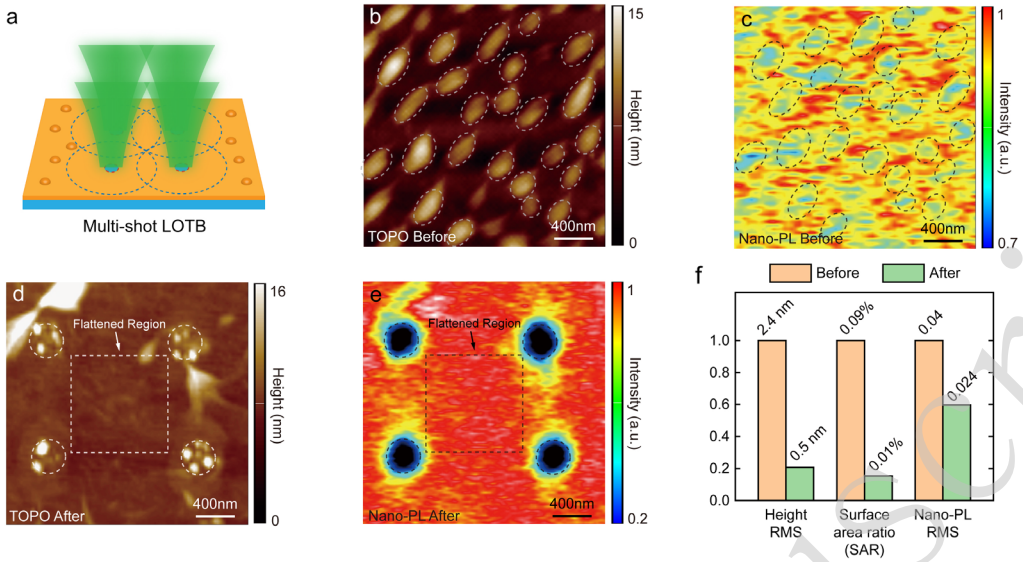

Figure 4. Multi-shot LOTB. (a) Schematic of the multi-shot LOTB with four lasers irradiating adjacent positions. (b) Topography and (c) nano-PL mapping images of a 1L-MoS_2 sample with nanobubbles. (d) AFM Topography and (e) nano-PL mapping images of the sample after four-shot LOTB with intensity of 101.9 mW/μm^2 and spot diameter of 0.3 μm. The dashed cycles spaced 1.5 μm apart indicate the irradiation points and sacrifice regions under laser irradiation, while the dashed rectangle indicates the flattened region of 1 μm×1 μm. (f) Surface roughness statistics of the flattened region before and after LOTB treatment.

In addition to the dual-beam cascaded LOTB, we can also further improve the effectiveness and control the position of the treatment area by multip-shot LOTB. As a demonstration in Fig. 4a, four laser beams are used to irradiate the sample in a square array in sequence, which avoids overheating or damage in the overlapping areas. Since each laser beam can affect a circular region centered around it, the overlapping regions in between can be controlled to realize a flattened region. As shown by the AFM topography images before and after multi-shot LOTB in Figs. 4b and 4d, the four irradiation spots (dashed circles in Figs. 4d-e) are spaced by 1.5 μm apart with power equal to 7.2 mW. The dashed rectangle indicates the flattened region of 1 μm×1 μm.

Accepted Manuscript

According to the surface roughness statistics results in Fig. 4f, the height RMS and SAR decrease by 80% and 89% after multi-shot LOTB, indicating that the flattening effect is significantly improved than that in the single-shot LOTB in Fig. 2g.

Experimental study of the optoelectronic properties of the treated region before and after LOTB is very important, but is difficult to implement at nanoscale due to the lack of experimental tool.[32] Fortunately, by applying a nano-PL microscopy that we have developed recently,[4] super-resolution mapping of the excitonic property of the TMD film can be performed in ambient condition with an ultra-high spatial resolution of 10 nm (see details of nano-PL in Methods section). As shown in Fig. 4c, before laser irradiation, the PL emission is weakened in nanobubble areas (dashed black circles in Fig. 4c), which is caused by the dielectric environment induced doping effect in nanobubbles.[33] In contrast, after multi-shot LOTB, the optoelectronic property in the flattened region (dashed black rectangle in Fig. 4e) is even and intact due to the elimination of nanobubbles, as verified by the RMS reduction in Fig. 4f. The above results show the effectiveness of LOTB to eliminate nanobubbles and improve the quality of 2D material based devices.

Conclusion

In this work, we have reported an all-optical LOTB method that can effectively and efficiently flatten 1L-TMDs with nanobubbles at a time scale of ~50 ms. By theoretical simulation and experimental investigation of the sample topography during LOTB, the optothermal dynamics dominated by phase transition are revealed. By applying LOTB, nanobubbles in transferred 1L-MoS_2 samples were effectively eliminated with the surface roughness decreased by 71% and 79% in topography RMS and SAR, respectively. In addition to single-shot LOTB, we have developed dual-beam cascaded LOTB and multi-shot LOTB to expand the flattened region and improve the elimination efficiency. Moreover, the optoelectronic properties of the treated sample have been studied by confocal PL microscopy, nano-PL microscopy, and Raman spectroscopy,

Accepted Manuscript

which show that the treated regions are intact. Future studies could focus on the electrical and thermal performance of devices based on 2D material-based after LOTB treatment. To meet the fabrication demand of 2D material-based semiconductor devices, In addition to the optical field engineering, the scalability of the proposed method could be further enhanced by incorporating conventional thermal treatment, such as global annealing via a heating stage. And the multi-shot LOTB treated nanobubble-free area can be as large as possible by aligning the sacrifice regions with the lines of wafer dicing in future manufacture.[34] Also, the throughput of the LOTB method can be greatly increased by employing multifocal parallel irradiation strategies, such as using microlens arrays. Our study not only reveals the formation dynamics of nanobubbles and explores how they change under laser irradiation, but also provides an efficient and promising post-treatment tool for nanodefect repair, which may play important role in next-generation semiconductor industry.

Accepted Manuscript

Materials and Methods

Preparation of the 1L-MoS_2 sample by wet transfer. Commercial 1L-MoS_2 films are grown by CVD on Al_2O_3 substrates and then transferred to the desired substrates (here, glass coverslips) by KOH-based wet transfer method. Specifically, the 1L-MoS_2 sample on the initial substrate with polymethyl methacrylate (PMMA) is heated at 100 °C, and then immersed in 2 mol/L KOH solution for several hours until the PMMA film is separated from the substrate naturally. After that, the PMMA film is washed by deionized water for 3-5 times and transferred onto glass coverslip. Then the sample is left to dry naturally and heated at 80℃. Finally, to etch the PMMA, the sample is immersed in acetone for 3-5 times with 30 minutes for each time. The growth and transfer are both performed by 6Carbon Technology (Shenzhen).

LOTB system. The LOTB system is established based on an inverted microscope (IX81, Olympus). The puncture-beam comes from a CW 532 nm laser (MGL-III-532nm, CNI) with a maximum power of 150 mW passing through a dichroic mirror with a 535 nm cut-off (FF535-SDi01, Semrock) and is focused on the sample by a 1.4 NA oil-immersion objective lens (100x, Olympus) after spatial filtering through a 50 μm pinhole (P50K, Thorlabs). The flattening-beam comes from another laser (MGL-U-532nm, CNI) with a higher power of 1.5 W. A convex lens (f = 100 mm) is used to turn the laser beam into divergence to produce a large-scale spot at the focal plane of the microscope. Then, the two laser beams are combined in one optical path through a 10:90 beam splitter. An electronic shutter (GCI-73M, Daheng Optics) is used to control the laser on and off with open time (measured time from 50%) close to 10 ms. The system has a much lower cost and can be readily implemented as an extension to conventional optical microscopy or integrated into existing optical processing platforms, making it highly compatible with current laboratory and industrial setups.

AFM and nano-PL characterization. AFM and nano-PL characterizations are performed based on a home-built near-field microscope setup combining an AFM

Accepted Manuscript

(NTEGRA, NT-MDT) and an inverted microscope. Both the AFM probe and the sample stage are mounted on high-precision three-dimensional piezoelectric scanners (NX100, NT-MDT), with which the focused beam can be aligned with the probe and perform the sample mapping. For nano-PL characterization, the near-field PL signal under the apex is modulated by an AFM probe working in tapping mode. Then the PL signal detected by the PMT is sent to a lock-in amplifier (HF2LI, Zurich Instruments) and demodulated to extract super-resolution signal in the near field. The control of the whole system is operated with an AFM controller. The probes used in the system are commercial silicon AFM probes (NSG01, ScanSens), and the mapping results are all carried out by raster scans from left to right.

Spectral measurements. The micro-PL and Raman spectral measurements are conducted by using the same setup of the LOTB system. Under the excitation laser of 532 nm wavelength, the micro-PL and Raman signals of the sample can be collected by the same objective and filtered with a filter set including a 550 nm long-pass filter (FELH0550, Thorlabs) and a 700 nm short-pass filter (FESH0700, Thorlabs), and then acquired by a confocal Raman spectrometer (INVA, Renishaw) or a PMT (PMT1002, Thorlabs).

Acknowledgements

The authors acknowledge the financial support of the National Natural Science Foundation of China (62175121, 61960206003).

Author contributions

J.T.H., B.F.B., and H.B.S. conceived the idea. B.F.B., and H.B.S. supervised the work. J.T.H. designed and conducted the LOTB experiments. H.R.C. provided a mechanical analysis of nanobubbles. J.T.H., P.Y.F., J.Y.Z and Y.X.H. built the LOTB system with in-situ optical characterization. X.J.W., H.W.Z. and G.Y.H. provided a theoretical analysis of the optothermal and strain effect of the LOTB method. Y.C. and Y.W

Accepted Manuscript

performed ultra-fast laser experiments. J.T.H., B.F.B., and H.B.S. wrote the manuscript with all authors' contributions. All authors participated in the discussion of the results and wrote the manuscript.

Data availability

All data are available from the corresponding authors upon reasonable request.

Conflict of interest

The authors declare no competing interests.

Reference

1. Mak, K.F. et al. Atomically Thin MoS_2: A New Direct-Gap Semiconductor. *Physical Review Letters* **105**, 136805 (2010).
2. Xia, Y. et al. 12-inch growth of uniform MoS_2 monolayer for integrated circuit manufacture. *Nature Materials* **22**, 1324-1331 (2023).
3. Khestanova, E. et al. Universal shape and pressure inside bubbles appearing in van der Waals heterostructures. *Nature Communications* **7**, 12587 (2016).
4. Huang, J.-T. et al. Super-Resolution Exciton Imaging of Nanobubbles in 2D Semiconductors with Near-Field Nanophotoluminescence Microscopy. *ACS Nano* **18**, 272-280 (2024).
5. Mak, K.F. et al. Control of valley polarization in monolayer MoS_2 by optical helicity. *Nature Nanotechnology* **7**, 494-498 (2012).
6. Novoselov, K.S. et al. 2D materials and van der Waals heterostructures. *Science* **353**, aac9439 (2016).
7. Zhang, T. et al. Clean Transfer of 2D Transition Metal Dichalcogenides Using Cellulose Acetate for Atomic Resolution Characterizations. *ACS Applied Nano Materials* (2019).
8. Liu, Z. et al. Strain and structure heterogeneity in MoS_2 atomic layers grown by chemical vapour deposition. *Nature Communications* **5**, 5246 (2014).

Accepted Manuscript

9. Liang, Q. et al. Defect Engineering of Two-Dimensional Transition-Metal Dichalcogenides: Applications, Challenges, and Opportunities. *ACS Nano* **15**, 2165-2181 (2021).

10. Sanchez, D.A., Dai, Z. & Lu, N. 2D Material Bubbles: Fabrication, Characterization, and Applications. *Trends in Chemistry* **3**, 204-217 (2021).

11. Sanchez, D.A. et al. Mechanics of spontaneously formed nanoblisters trapped by transferred 2D crystals. *Proceedings of the National Academy of Sciences* **115**, 7884-7889 (2018).

12. Buscema, M. et al. The effect of the substrate on the Raman and photoluminescence emission of single-layer MoS_2. *Nano Research* **7**, 561-571 (2014).

13. Huang, J. et al. Super-resolved discrimination of nanoscale defects in low-dimensional materials by near-field photoluminescence spectral imaging. *Optics Letters* **47**, 4227-4230 (2022).

14. Shabani, S. et al. Ultralocalized Optoelectronic Properties of Nanobubbles in 2D Semiconductors. *Nano Letters* **22**, 7401-7407 (2022).

15. Zhang, D. et al. Reconstructing Local Profile of Exciton–Emission Wavelengths across a WS_2 Bubble beyond the Diffraction Limit. *ACS Nano* **14**, 6931-6937 (2020).

16. Liu, H., Zhao, J. & Ly, T.H. Clean Transfer of Two-Dimensional Materials: A Comprehensive Review. *ACS Nano* **18**, 11573-11597 (2024).

17. Lee, H.Y. et al. Strong and Localized Luminescence from Interface Bubbles Between Stacked hBN Multilayers. *Nature Communications* **13**, 5000 (2022).

18. Rosenberger, M.R. et al. Nano-"Squeegee" for the Creation of Clean 2D Material Interfaces. *ACS Applied Materials & Interfaces* **10**, 10379-10387 (2018).

19. Khestanova, E. et al. Universal shape and pressure inside bubbles appearing in van der Waals heterostructures. *Nature Communications* **7**, 12587 (2016).

Accepted Manuscript

20. Pizzocchero, F. et al. The hot pick-up technique for batch assembly of van der Waals heterostructures. *Nature Communications* **7**, 11894 (2016).

21. Rafiee, J. et al. Wetting transparency of graphene. *Nature Materials* **11**, 217-222 (2012).

22. Velasco, S., Román, F.L. & White, J.A. On the Clausius–Clapeyron Vapor Pressure Equation. *Journal of Chemical Education* **86**, 106 (2009).

23. Corti, H.R. et al. Structure and dynamics of nanoconfined water and aqueous solutions. *The European Physical Journal E* **44**, 136 (2021).

24. Lanzillo, N.A. et al. Temperature-dependent phonon shifts in monolayer MoS_2. *Applied Physics Letters* **103** (2013).

25. Castellanos-Gomez, A. et al. Local Strain Engineering in Atomically Thin MoS_2. *Nano Letters* **13**, 5361-5366 (2013).

26. Li, Z. et al. Efficient strain modulation of 2D materials via polymer encapsulation. *Nature Communications* **11**, 1151 (2020).

27. Wang, X. et al. Effects of solvents and polymer on photoluminescence of transferred WS_2 monolayers. *Journal of Vacuum Science & Technology B* **37** (2019).

28. Ma, C., Chen, Y. & Chu, J. Time-Dependent Pinning of Nanoblisters Confined by Two-Dimensional Sheets. Part 1: Scaling Law and Hydrostatic Pressure. *Langmuir* **39**, 701-708 (2023).

29. Jiang, J.-W., Park, H.S. & Rabczuk, T. Molecular dynamics simulations of single-layer molybdenum disulphide (MoS2): Stillinger-Weber parametrization, mechanical properties, and thermal conductivity. *Journal of Applied Physics* **114** (2013).

30. Cai, Y. et al. Lattice vibrational modes and phonon thermal conductivity of monolayer MoS_2. *Physical Review B* **89**, 035438 (2014).

31. Bi, J. et al. Flat-top beam shaping and optimization based on a single aspheric lens. *Optics & Laser Technology* **183**, 112391 (2025).

Accepted Manuscript

ACCEPTED ARTICLE PREVIEW

32. Chen, X. et al. Modern Scattering-Type Scanning Near-Field Optical Microscopy for Advanced Material Research. *Advanced Materials* **31**, 1804774 (2019).

33. Chowdhury, T. et al. Modulation of trion and exciton formation in monolayer WS_2 by dielectric and substrate engineering. *2D Materials* **8**, 045032 (2021).

34. Singh, J. et al. Growth of Wafer-Scale Single-Crystal 2D Semiconducting Transition Metal Dichalcogenide Monolayers. *Advanced Science* **11**, 2307839 (2024).

Accepted Manuscript